Nuclear Engineering and Technology 54 (2022) 177–185

Contents lists available at ScienceDirect

Nuclear Engineering and Technology

journal homepage: www.elsevier.com/locate/net

Original article

Analyses of hydrogen risk in containment filtered venting system using MELCOR

Gi Hyeon Choi [a], Dong-Wook Jerng [a, *], Tae Woon Kim [b]

[a] School of Energy Systems Engineering, Chung-Ang University, 84, Heukseok-ro, Dongjak-gu, Seoul, Republic of Korea
[b] Korea Atomic Energy Research Institute, 98-111, Daedeok-daero, Yuseong-gu, Daejeon, Republic of Korea

ARTICLE INFO

Article history:
Received 30 July 2020
Received in revised form
29 July 2021
Accepted 30 July 2021
Available online 31 July 2021

Keywords:
Containment filtered venting system
Hydrogen risk
Severe accident

ABSTRACT

Hydrogen risk in the containment filtered venting system (CFVS) vessel was analyzed, considering operation pressure and modes with the effect of PAR and accident scenarios. The CFVS is to depressurize the containment by venting the containment atmosphere through the filtering system. The CFVS could be subject to hydrogen risk due to the change of atmospheric conditions while the containment atmosphere passes through the CFVS. It was found that hydrogen risk increased as the CFVS opening pressure was set higher because more combustible gases generated by Molten Core Concrete Interaction flowed into the CFVS. Hydrogen risk was independent of operation modes and found only at the early phase of venting both for continuous and cyclic operation modes. With PAR, hydrogen risk appeared only at the 0.9 MPa opening pressure for Station Black-Out accidents. Without PAR, however, hydrogen risk appeared even with the CFVS opening set-point of 0.5 MPa. In a slow accident like SBO, hydrogen risk was more threatening than a fast accident like Large Break Loss-of-Coolant Accident. Through this study, it is recommended to set the CFVS opening pressure lower than 0.9 MPa and to operate it in the cyclic mode to keep the CFVS available as long as possible.

1. Introduction

The containment filtered venting system (CFVS) is a passive safety system. The CFVS filters the radioactive material in the containment atmosphere and vents the gas to maintain the integrity of the containment building [1]. There were installed in European nuclear power plants (NPPs) after the Chernobyl NPP accident. After the Fukushima Daiichi NPP accident, The CFVS installation was considered worldwide [2]. In Korea, a high speed sliding pressure venturi (HSSPV) scrubber system developed by Areva was once installed in Wolsong NPP unit 1 [3]. This system is a wet-type CFVS that consists of two pipes and a vessel, as shown in Fig. 1. When the pressure in the containment building reaches a set point, a valve in the front pipe is opened and the containment building atmosphere flows into the CFVS. A scrubbing pool and metal fiber filter prevent the emission of radioactive materials, and the gas mixture is discharged into the environment [4]. Studies have demonstrated the utility of the CFVS for depressurizing the containment building and filtering radioactive materials [5–7].

In an accident, combustible gases such as hydrogen and carbon monoxide (CO) are generated by cladding oxidation and molten corium concrete interaction (MCCI) [8,9]. The combustible gases can explode and damage the containment building. A hydrogen explosion at the Fukushima Daiichi NPP breached the containment building [10]. Such explosions must be avoided when operating NPPs. To prevent hydrogen explosions, passive autocatalytic recombiners (PARs), which reduce the hydrogen content via recombination, and hydrogen igniters have been introduced [11].

The CFVS could be also subject to hydrogen risk. The CFVS releases the containment atmosphere into the environment; thus, the gas mixture, including combustible gases, flows into the CFVS before exiting to the environment. When the containment atmosphere passes the CFVS vessel, the steam condenses; this increases the fraction of combustible gas, can give rise to hydrogen risk in the CFVS vessel. This hydrogen risk is obviously dependent on the containment atmosphere conditions which are affected by the CFVS operating strategy. For example, if the CFVS is set to open at a higher pressure, the containment atmosphere may accumulate more combustible gas before the initiation of the CFVS operation, resulting in a higher hydrogen risk not only in the containment but also in the CFVS vessel.

* Corresponding author.
E-mail address: dwjerng@cau.ac.kr (D.-W. Jerng).

https://doi.org/10.1016/j.net.2021.07.046

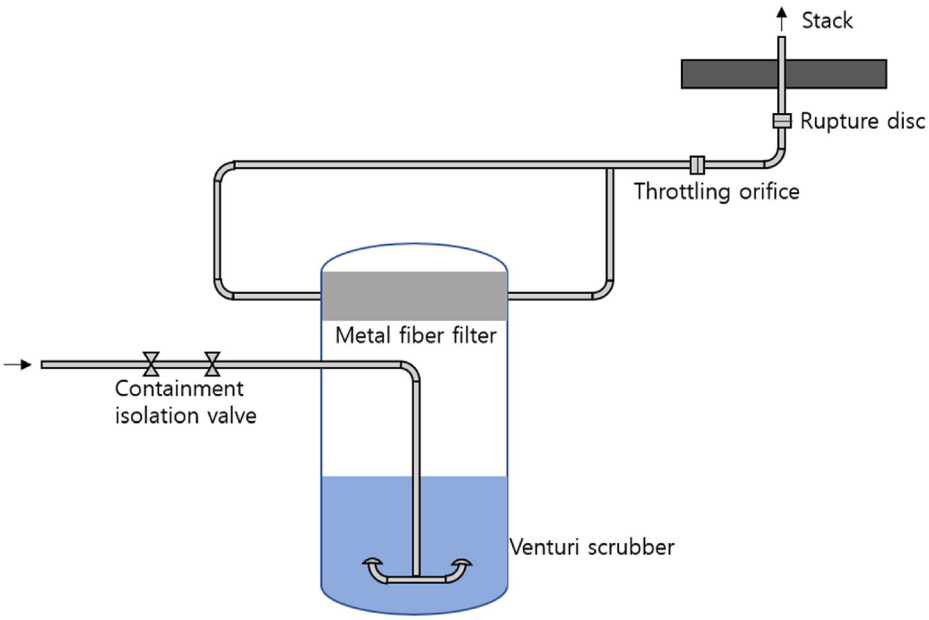

Fig. 1. Schematic diagram of a high-speed sliding pressure venting.

Y. S. Na et al. demonstrated that hydrogen risk could exist in the CFVS vessel during an early phase of its operation [12]. However, their analysis did not consider the effects of the CFVS opening pressure, operation mode, PAR, or CO generation due to MCCI. M. Löffler and M. Braun found that the early venting of the CFVS would pose hydrogen risk, but they did not consider late venting cases [13]. Z. Ma et al. studied a horizontal type CFVS using a CFD code and they found that there would be hydrogen risk [14]. They suggested nitrogen injection to inert the CFVS vessel atmosphere to avoid hydrogen risk. There has been, however, little study regarding the effects of the CFVS operating strategy, PAR, and accident scenarios on hydrogen risk in detail. As aforementioned, the combustible gas concentration in the containment atmosphere is dependent on the CFVS operating strategy, i.e., the delayed opening of the CFVS will result in a higher concentration of combustible gas in the containment atmosphere vented to the CFVS vessel. And also, a cyclic and continuous operating strategy may affect hydrogen risk in the CFVS vessel. PAR reduces the hydrogen concentration, thereby lowering the probability of hydrogen explosion in the CFVS vessel as well as in the containment building. In addition, CO should be considered as it is combustible like hydrogen. Therefore, hydrogen risk in the CFVS vessel is comprehensibly addressed in this paper with regard to the CFVS operating strategies, considering PAR and the effect of CO.

The contents of the paper are as follows. Section 2 presents the analysis model, accident scenario, CFVS operating strategy, and hydrogen risk estimating method. Section 3 presents the results of the hydrogen risk analyses. And in Section 4, finally, conclusions are summarized.

2. Analysis methods

2.1. Model description

In this study, MELCOR 1.8.6 was used to analyze the hydrogen risk in the CFVS vessel in various accident scenarios [15]. A 1000-MW_e two-loop pressurized light water reactor, OPR-1000, was modeled for the analyses. The reactor coolant system (RCS) in the model consists of a reactor, a pressurizer, two steam generators, two hot legs, four reactor coolant pumps, and four cold legs. A safety injection tank (SIT) connected to each cold leg [16]. Fig. 2 is a schematic diagram of the RCS model. Table 1 summarizes the design parameters for OPR-1000 and the normal operating conditions of the model [17]. Fig. 3 shows the nodalization of the containment building and the CFVS. Nodalization sensitivity was also carried out with a more detailed containment nodalization with 10 nodes in the upper compartment region of the containment instead of three nodes as shown in Fig. 3. No difference in hydrogen concentration was observed. Therefore, we used the model shown in Fig. 3 for the analyses presented here. It should be noted that the hydrogen distribution was found uniform in the containment except during the early phase of the accident when hydrogen is ejected into the containment together with molten core debris. Thus, hydrogen distribution in the containment was not an issue for the CFVS hydrogen risk analysis as the CFVS begins its operation at least 24 h after the accidents when the containment pressure reaches an opening set-point which is shown in Figs. 4 and 5. This observation of nodalization sensitivity and uniformity of hydrogen was also reported in Ref. [18] in which A. Sartmadjiev reported that the hydrogen distribution was not affected by a node size and became almost uniform within the containment. PARs were modeled inside the containment building. The CFVS was modeled with a pipe connecting to the upper compartment of the containment, outlet pipe to the external environment, and two volumes; upper and lower regions of the CFVS vessel which was 6.5 m in height and 3 m in diameter. The CFVS vessel was filled with water up to 3 m from the bottom for the scrubbing purpose. The sparger model provided in the MELCOR code was applied at the end of the inlet pipe submerged in the CFVS pool.

2.2. Description of accident scenarios

In this paper, a large break loss of coolant accident (LBLOCA) and station blackout (SBO) were selected as the relatively fast and slow accident conditions, respectively. For conservative analyses, we assumed that only SIT could be used for accident mitigation, i.e., all active emergency core cooling systems, such as the containment spray system and safety injection system, were not available.

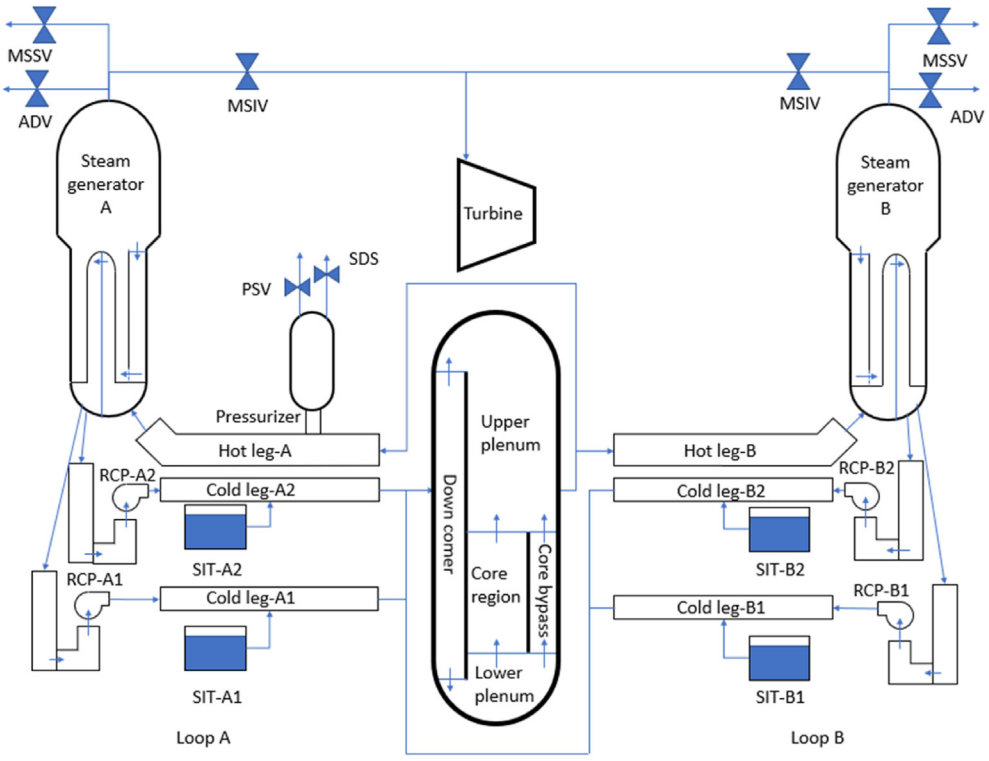

Fig. 2. MELCOR nodalization for reactor coolant system model.

Table 1
Comparison of the OPR-1000 FSAR data and normal operating conditions of the MELCOR model.

Parameter		Unit	FSAR data	MELCOR normal operating conditions
Thermal output		MW_{th}	2825	2825
Temperature	Cold leg	°C	295.8	303.44
	Hot leg	°C	327.3	333.26
	RCS average	°C	311.6	318.35
	SIT	°C	48.9	59.99
Pressure		MPa	15.82	14.91
Mass flow rate		kg/s	15,306	15,370
Coolant volume	RCS	m^3	287.4	281.56
	Pressurizer	m^3	25.63	27.69
	SIT	m^3	For each 52.6	For each 52.60

FSAR, final safety analysis report; RCS, reactor coolant system; SIT, safety injection tanks.

Table 2 summarizes the sequence of the major events in the two accident scenarios.

In the SBO, the RCS pressure was appropriately maintained for 1.0 h by the SG cooling. As the SG inventory was depleted, the RCS pressure rapidly increased, and eventually, the pressurizer safety valve (PSV) opened at 1.4 h. The RCS coolant was, then, discharged to the containment atmosphere through PSV, resulting in the containment pressure increase. The cladding oxidation occurred at 2.38 h due to the RCS inventory depletion. Thereafter, the reactor vessel failed at 4.44 h due to the molten corium. The molten corium fell into the reactor cavity filled with coolant and this led to the release of hydrogen and CO via MCCI. The reactor cavity dried-out at 44.9 h due to the decay heat of the molten corium and thereafter MCCI was accelerated. At 72 h, the containment pressure reached 1.01 MPa which was the containment failure condition.

On the other hand, in the LBLOCA, a large amount of the RCS coolant was discharged to the containment through the broken loop, which rapidly increased the containment pressure. Due to the rapid loss of RCS inventory, the cladding oxidation occurred at 0.39 h. Later, the reactor vessel failed at 2.19 h, and the molten corium was injected into the reactor cavity, which triggered the MCCI. The cavity dried-out at 36.31 h. At 55.1 h, the containment pressure reached 1.01 MPa at which the containment failure was assumed to occur. This difference in accident sequences between SBO and LBLOCA could affect the conditions of the containment atmosphere flowing into the CFVS.

2.3. Description of the CFVS operating strategies

The CFVS has two operating modes: continuous and cyclic. In the continuous operation mode, The CFVS operates without closing, i.e., the CFVS remains open once operation commences. In the cyclic operation mode, The CFVS repeatedly opens and closes according to set points. The cyclic operation is known to have advantages with respect to decontamination performance, especially in view of scrubbing pool depletion [19] and noble gas emission [20].

In this study, we considered both operating modes, and CFVS

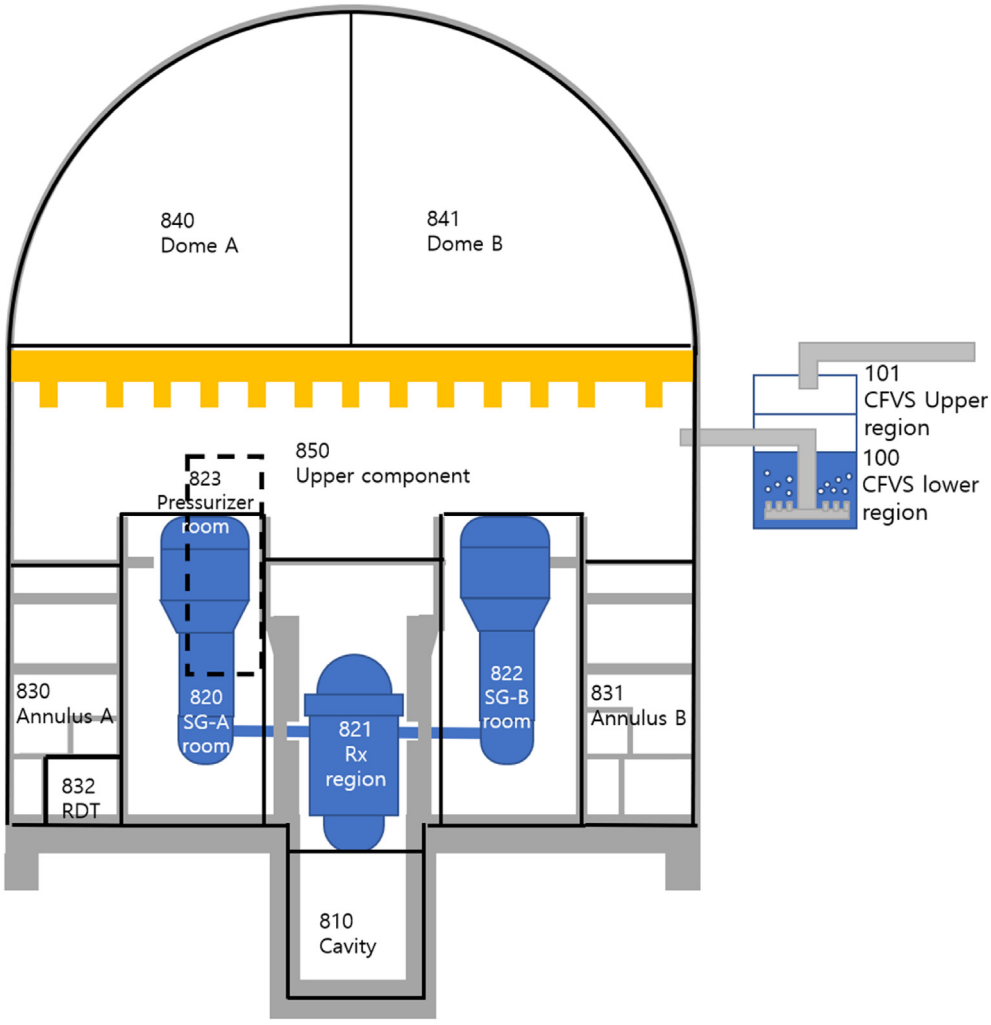

Fig. 3. MELCOR nodalization for containment and containment filtered venting system model.

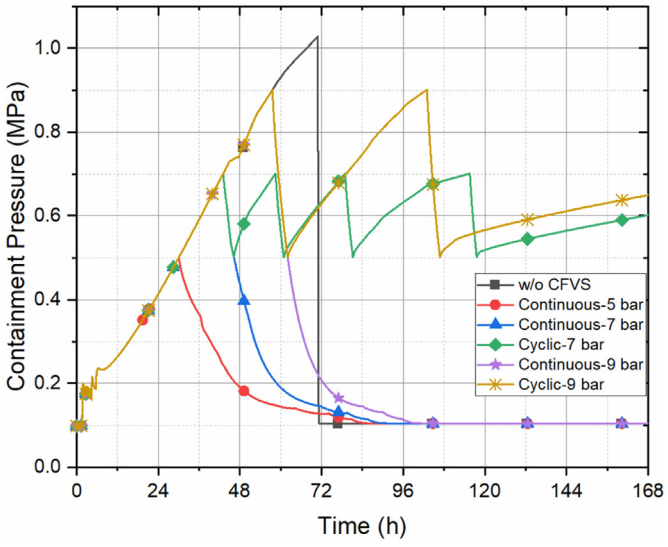

Fig. 4. Pressure behavior in containment building according to the CFVS operation strategies under the SBO scenario.

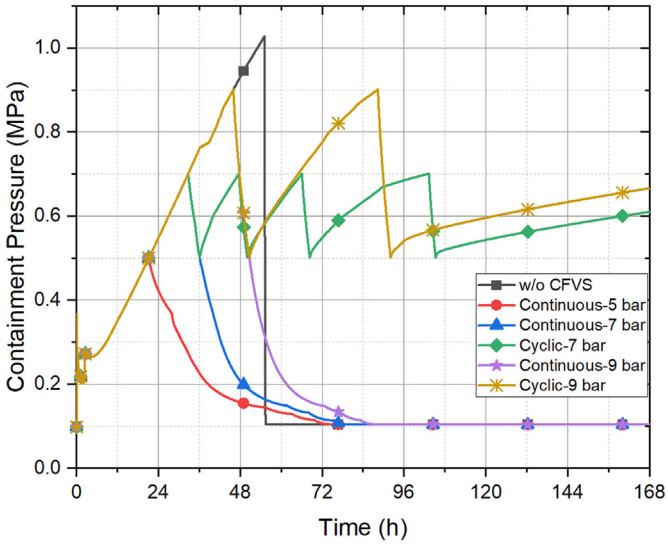

Fig. 5. Pressure behavior in containment building according to the CFVS operation strategies under the LBLOCA scenario.

Table 2
Comparison of the accident sequence for station blackout and large break loss of coolant accident.

Event	Time	
	SBO	LBLOCA
Accident occurrence	0	0
Reactor shutdown	0	0
Fuel uncovery	1.69 h	0.03 s
Cladding oxidation	2.38 h	0.39 h
SIT operation	4.55 h	14.4 s
Reactor vessel failure	4.44 h	2.19 h
Cavity dry out	44.90 h	36.31 h
MCCI acceleration	49.33 h	41.00 h
Containment building failure without the CFVS[a]	70.92 h	55.14 h

[a] The containment failure was assumed to occur at 1.01 MPa that S.-W. Lee et al. suggested with 5 % probability and 95 % confidence level [20].

opening pressures set to range from 0.5 to 0.9 MPa, which are the design pressure and the pressure 10% less than the failure pressure of the containment building, respectively. Three different pressures were chosen as opening set-points: 0.5, 0.7, and 0.9 MPa. In cyclic operating mode, the CFVS closed at 0.5 MPa and opened at the predetermined set-point. Table 3 summarizes the operating strategies of the CFVS analyzed. Fig. 4 shows the pressure in the containment building according to the operating strategies under the SBO scenario. The pressure inside the containment building reached 0.5, 0.7, and 0.9 MPa at 30.1, 43.1, and 57.9 h, respectively. In the studies of T. W. Kim et al. [21] and Y. S. Na et al. [22], a similar trend of the containment pressure was observed. In the cyclic operating mode, the CFVS operated 4 times and 2 times for 0.7 and 0.9 MPa set-points, respectively. Fig. 5 shows the containment pressure during LBLOCA. At 21.4, 32.7, and 45.7 h after LBLOCA, the pressure inside the containment building reached 0.5, 0.7, and 0.9 MPa, respectively. For the cyclic operating mode, the CFVS operated 4 times and 2 times for 0.7 and 0.9 MPa set-points, respectively as well. Table 4 summarizes the sequence of events.

To determine the effective time of the CFVS operation, the scrubbing pool inventory was analyzed, as shown in Figs. 6 and 7. Fig. 6 shows the CFVS scrubbing pool inventory under SBO scenarios. The pool inventory increased due to the steam condensation at the opening of the CFVS and then decreased due to the decay heat of radioactive materials. In the continuous operating mode, the scrubbing pool dried out at 58.8, 67.1, and 83.2 h after the accident for the CFVS opening pressure of 0.5, 0.7, and 0.9 MPa, respectively. In the cyclic operating mode, the scrubbing pool inventory lasted longer. For the CFVS opening pressure of 0.7 and 0.9 MPa with a closing pressure of 0.5 MPa, the scrubbing pool dried out at 128.3 and 119.3 h after the accident, respectively. Fig. 7 shows the CFVS scrubbing pool inventory under LBLOCA scenarios. In the continuous operating mode, the scrubbing pool dried out at 48.0, 60.1, and 77.0 h after the accident for the CFVS opening pressure of 0.5, 0.7, and 0.9 MPa, respectively. In the cyclic operating mode, the scrubbing pool dried out at 113.6 and 143.4 h for the CFVS opening pressure of 0.7 and 0.9 MPa, respectively. Table 5 summarizes the scrubbing pool depletion time analysis.

Table 3
Summary of the CFVS operation strategies to be considered for comparison analyses.

Operation strategy	Opening pressure (MPa)	Closing pressure (MPa)
Continuous venting	0.5	N/A
	0.7	N/A
	0.9	N/A
Cyclic venting	0.7	0.5
	0.9	0.5

2.4. Assessment of the hydrogen risk

For a hydrogen explosion to occur, the concentration of hydrogen must be within a specific range [23]. The Shapiro diagram is a popular method to assess the hydrogen-burning and detonation conditions. It shows the flammability limits of hydrogen-burning and explosion in the mixtures of air, steam, and hydrogen [24]. When an accident occurs, the atmosphere of the containment building contains CO, carbon dioxide (CO_2), air, steam, and hydrogen. Among them, combustible gases are hydrogen and CO. To draw a Shapiro diagram, the total volume fraction of combustible gases is obtained by combining the volume fractions of hydrogen and CO. However, CO has a lower flammability limit approximately twice that of hydrogen. It is known that the contribution of CO on flammability is about half of hydrogen [15,23]. Therefore, the volume fraction of the combustible gases is calculated as a sum of hydrogen and 0.5 times CO. If PAR is in use, the volume fraction of air is changed as PAR removes hydrogen together with oxygen in the air. To calculate the effect of PAR operation on air fraction, the air is considered to be decomposed as 21 % oxygen and 79 % nitrogen. The change of the air volume fraction in the containment is calculated by subtracting the volume fraction of oxygen combined with hydrogen from the initial amount of air [24]. The amount of hydrogen removed by PAR is calculated by a correlation embedded in MELCOR. For example, if 1 mol of hydrogen is removed by PAR, then, 0.5 mol of oxygen is removed from the air. Thus, the air mass is decreased as the oxygen mass is decreased because air is composed of oxygen and nitrogen. And then, there is nitrogen left-over due to the reduction of the air mass. This nitrogen surplus is added to the inert gases. The inert gases in the Shapiro diagram, therefore, consist of steam, and CO_2, As the inerting effectiveness of nitrogen is approximately 80% of that of other inert gases, e.g., CO_2 and steam [15,25]. Therefore, the contribution of the nitrogen is reduced by 20%, considering this inerting effectiveness. Table 6 summarizes the formulas to calculate the volume fractions of air, inert and combustible gases in the Shapiro diagram.

3. Results and discussions

To analyze the hydrogen risk associated with the CFVS operation, the Shapiro diagram is utilized which is a ternary plot composed of 3 axes; air, inert gas, and combustible gas. The baseline of the Shapiro diagram represents the volume fraction of combustible gas, left and right hypotenuses represent the volume fractions of air and inert gas, respectively. To read the Shapiro-diagram, draw lines parallel to each hypotenuse at a given point and check the intersection of the drawn lines with the each hypotenuse of the triangle; the air portion is at the intersection between the left hypotenuse and a line parallel to the base of the triangle, the steam portion is at the intersection between the right hypotenuse and a line parallel to the left hypotenuse, and the hydrogen portion is at the intersection between the base line and a line parallel to the right hypotenuse. The flammability limits of a combustible gas mixed in the air and inert gas are easily identified by the Shapiro diagram [24].

The Shapiro diagram shown in Fig. 8 indicates the change of air, combustible, and inert gas volume fractions in the CFVS vessel according to the CFVS operating modes for SBO scenarios. For the CFVS opening pressure of 0.5 or 0.7 MPa, the combustible gas volume fraction never exceeds 5% which is the burnable limit until the inert gas volume fraction exceeds 60%, resulting in no hydrogen risk, regardless of a continuous or cyclic operation mode. For both cyclic and continuous operation modes with the CFVS opening pressure of 0.9 MPa, the combustible gas volume fraction exceeds

Table 4
CFVS operation sequence of events.

Accident scenario	Opening pressure (MPa)	Continuous operation	Cyclic operation	
		Opening time (h)	Opening time (h)	Closing time (h)
SBO	0.5	30.1		
	0.7	43.1	43.1	46.2
			58.2	60.9
			79.3	81.1
			115.6	117.6
	0.9	57.9	57.9	62.1
			103.0	106.8
LBLOCA	0.5	21.4		
	0.7	32.7	32.7	36.1
			47.4	50.1
			66.1	68.4
			103.3	105.3
	0.9	45.7	45.7	50.7
			88.3	92.1

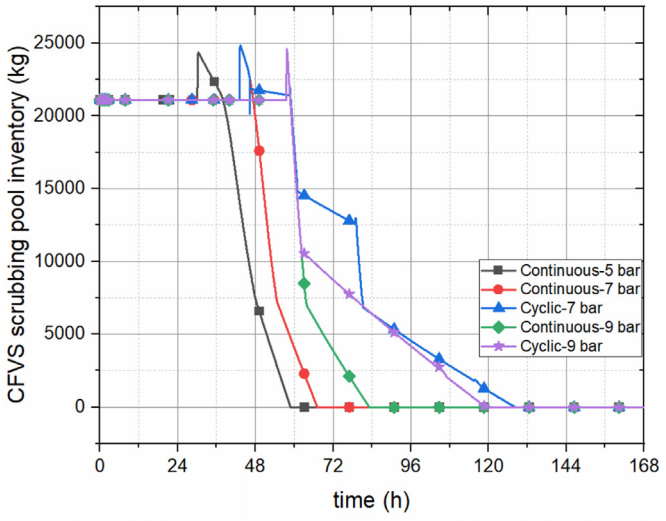

Fig. 6. CFVS scrubbing pool inventory behavior according to the CFVS operation strategies under the SBO scenario.

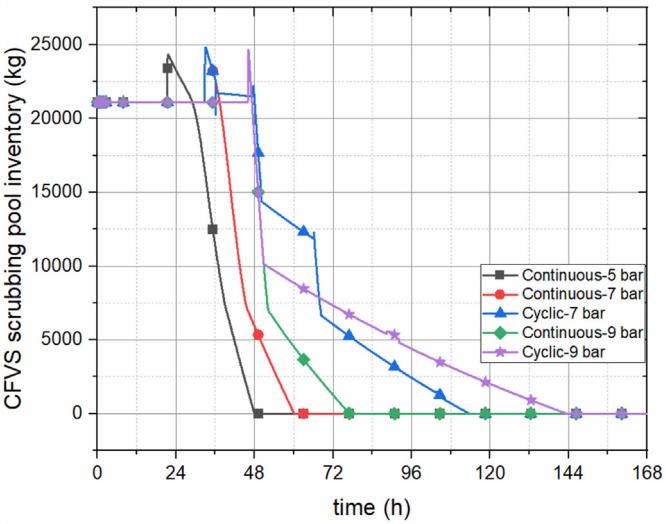

Fig. 7. CFVS scrubbing pool inventory behavior according to the CFVS operation strategies under the LBLOCA scenario.

5% at the beginning of the CFVS operation, and the CFVS atmosphere condition enters the burnable region but escapes out of the burnable limit as the inert gas concentration increases while the combustible gas and air concentration decrease. Fig. 9 shows the change of gas and air volume fractions alone the time from the initiation of the CFVS operation. In the beginning, the CFVS atmosphere condition is at Point A in Figs. 8 and 9. Note that the humidity of the CFVS vessel atmosphere on standby condition was assumed to be 90% at 34 °C. For the 0.9 MPa opening pressure case, the CFVS atmosphere condition passes the burnable limit line which is marked as Point B in Figs. 8 and 11, 11 s after the CFVS operation as the combustible gas concentration increases from 0 to 5.0%. And the maximum combustible gas concentration reaches 5.9% at 28 s. At 96 s, the CFVS vessel atmosphere condition exits from the burnable region which is marked as Point C in Figs. 8 and 9, because the combustible gas and air concentration decrease while the inert gas, which is mostly steam, continuously increases. The reason that the CFVS vessel atmosphere condition with the opening set-point of 0.9 MPa was more shifted to the left than that of 0.5 or 0.7 MPa is that the combustible gas concentration in the containment is higher due to MCCI for the 0.9 MPa opening pressure case. After Point C, in the continuous operating mode, the combustible gas concentration was increased a little at the end of operation as indicated by Point D in Fig. 8 due to the generation of combustible gas by MCCI. In the cyclic operation mode, the CFVS vessel atmosphere condition moved toward the burnable limit line momentarily as indicated by Point E in Fig. 8, but did not reach the burnable limit line. This is because the CFVS vessel atmosphere is in highly inert conditions due to high steam concentration at the second and successive openings. It can be, therefore, concluded that the hydrogen risk would exist only briefly on the initiation of venting from 11 s to 96 s after the opening of the CFVS only if the CFVS opening pressure was set as 0.9 MPa.

For the LBLOCA cases, no hydrogen risk was found according to the Shapiro diagram analysis shown in Fig. 10. Regardless of opening pressures and operation modes the hydrogen concentration in the CFVS vessel never exceeded the burnable limit of 5% hydrogen concentration. As it was found in the SBO analysis, however, the 0.9 MPa opening case was closer to the burnable limit than the other cases because of the MCCI effect. Compared with the SBO cases, LBLOCA was found to have a lower hydrogen risk. This is because the time for the CFVS opening is faster for the LBLOCA cases due to the more rapid pressurization as seen in Figs. 4 and 5, thus, resulting in the smaller effect of MCCI at the time of the CFVS opening. The total combustible gas concentrations in the containment atmosphere at the initiation of the CFVS operation were 1.1%

Table 5
Comparison of the CFVS scrubbing pool depletion time according to the CFVS operating strategies for SBO and LBLOCA.

Accident scenario	Opening pressure (MPa)	CFVS scrubbing pool depletion time (h)	
		Continuous operation	Cyclic operation
SBO	0.5	58.83	
	0.7	67.14	128.31
	0.9	83.19	119.25
LBLOCA	0.5	48.00	
	0.7	60.17	113.58
	0.9	76.97	143.39

Table 6
Formula to calculate gas fractions in the Shapiro diagram.

Gas	Formula
Air[a]	$\frac{N_{O_2}}{0.21N_T}$
Inert gas[b]	$\frac{N_{CO_2}+N_{H_2O}+0.8\left(N_{N_2}-\frac{0.79}{0.21}N_{O_2}\right)}{N_T}$
Combustible gas[c]	$\frac{N_{H_2}+0.5N_{CO}}{N_T}$

N_i : volume fraction of gas component i.

$N_T = \frac{N_{O_2}}{0.21}+\left(N_{CO_2}+N_{H_2O}+0.8\left(N_{N_2}-\frac{0.79}{0.21}N_{O_2}\right)\right)+(N_{H_2}+0.5N_{CO})$

[a] Air is composed of 21 % oxygen and 79 % nitrogen and air volume fraction depends only on the oxygen volume fraction.

[b] Inert gases are composed of steam, CO_2, and excessive nitrogen with a 20% reduction in inerting effectiveness.

[c] The effectiveness of CO as a combustible gas is assumed to be a half of hydrogen.

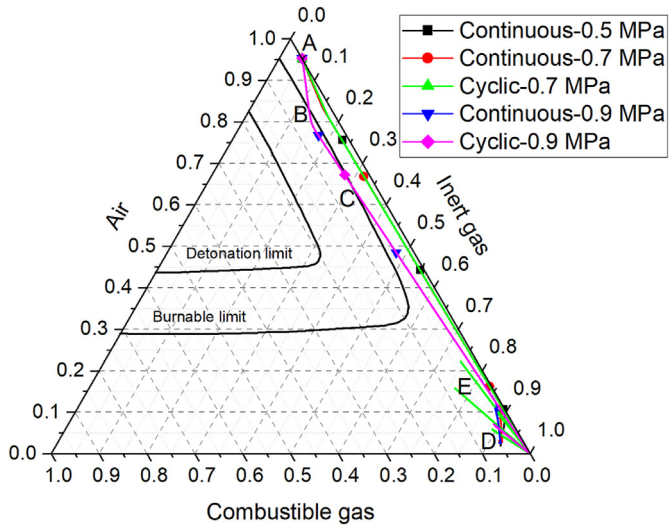

Fig. 8. Gas composition behavior in the CFVS vessel according to the CFVS operation strategies under SBO.

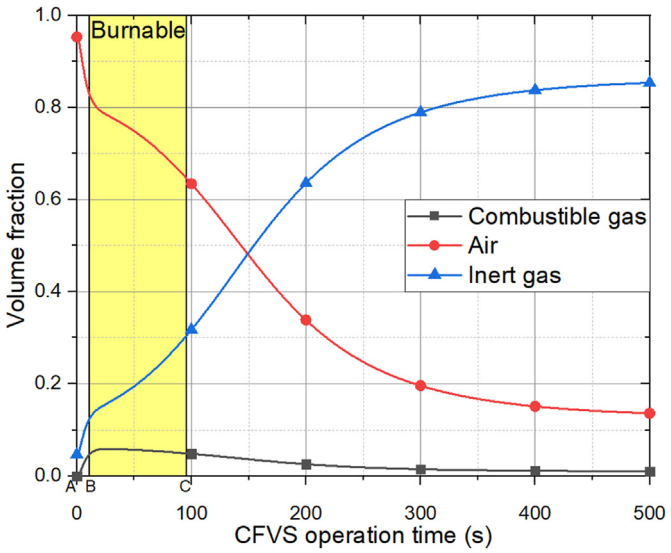

Fig. 9. Gas concentration behavior in the CFVS vessel after the CFVS operation under the SBO scenario with an opening pressure of 0.9 MPa.

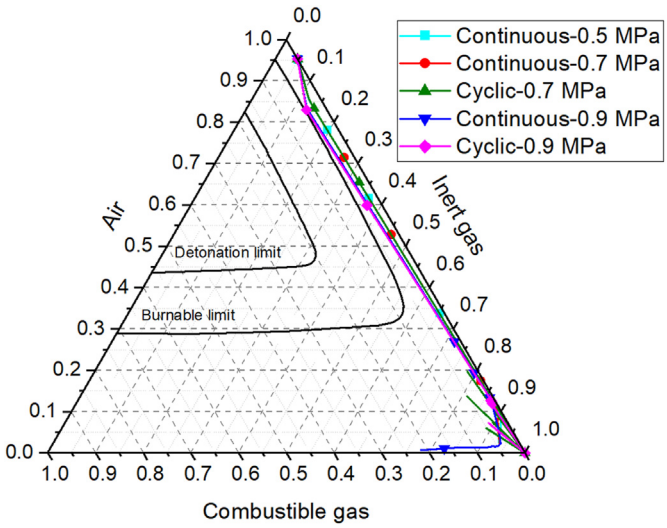

Fig. 10. Gas composition behavior in the CFVS vessel according to the CFVS operation strategies under LBLOCA.

and 0.90% for SBO and LBLOCA, respectively. Among them, the concentration of combustible gas due to MCCI was 0.91% and 0.64% for SBO and LBLOCA cases, respectively. As the combustible gas passed to the CFVS, the combustible gas concentration was increased, and then reached 5.8% and 4.3%, respectively, at the initiation of the CFVS operation.

The effect of PAR on the hydrogen risk in the CFVS vessel was analyzed with SBO and LBLOCA scenarios for continuous operation cases. Figs. 11 and 12 show the resulting Shapiro diagrams. It is clearly seen that the CFVS vessel atmosphere conditions shifted to the left compared to cases with PAR shown in Figs. 8 and 10. Without PAR, therefore, even 0.5 MPa opening pressure resulted in the hydrogen risk by making the CFVS vessel atmosphere condition trespass on the burnable limit for both SBO and LBLOCA, although there would be no hydrogen risk in the containment as seen in Fig. 13.

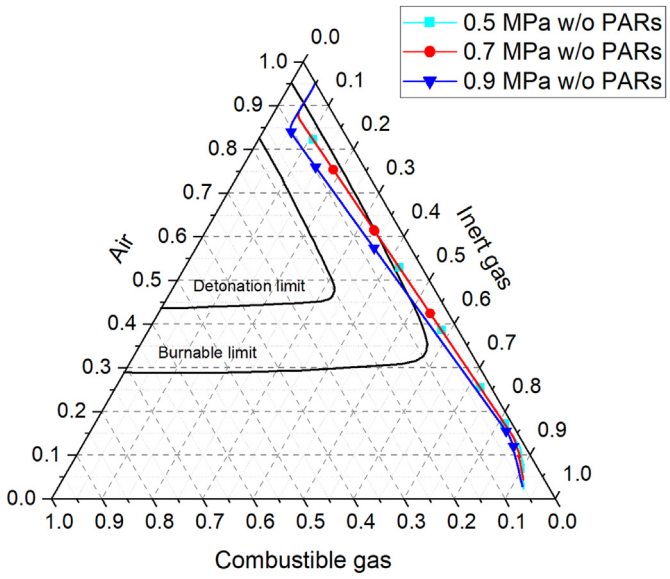

Fig. 11. Gas composition behavior in the CFVS vessel according to the CFVS operation pressure under SBO without PAR.

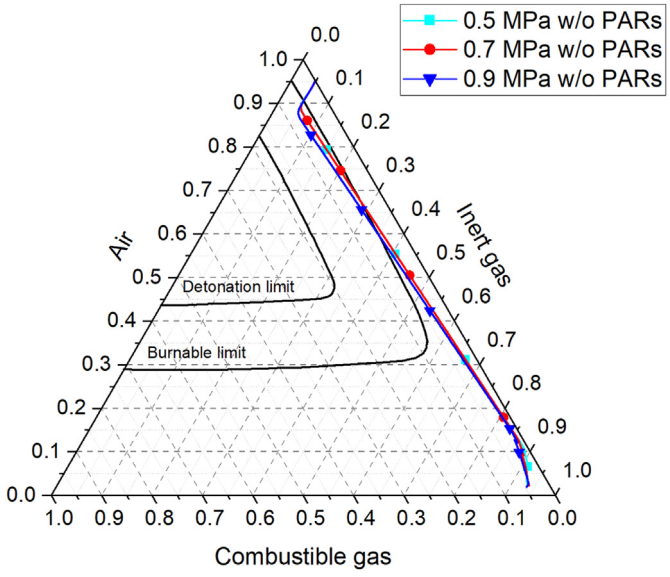

Fig. 12. Gas composition behavior in the CFVS vessel according to the CFVS operation pressure under LBLOCA without PAR.

4. Conclusion

In this study, the hydrogen risk in the CFVS vessel during SBO and LBLOCA was analyzed with regard to the operating pressure and mode, accident scenarios, and the installation of PAR.

Through this study, the main conclusions are as follows:

(1) The hydrogen risk depends on the CFVS opening pressure. For the CFVS opening pressure of 0.5 or 0.7 MPa with PARs in the containment, hydrogen risk did not appear for either SBO or LBLOCA, regardless of operation modes. For the CFVS opening pressure of 0.9 MPa, the combustible gas volume fraction in the CFVS vessel increased due to the combustible gas generated by MCCI, resulting in hydrogen risk. Therefore, it can be concluded that a higher CFVS opening pressure may result in a higher hydrogen risk. Therefore, it is recommended that the opening pressure of the CFVS should be set lower than 0.9 MPa.

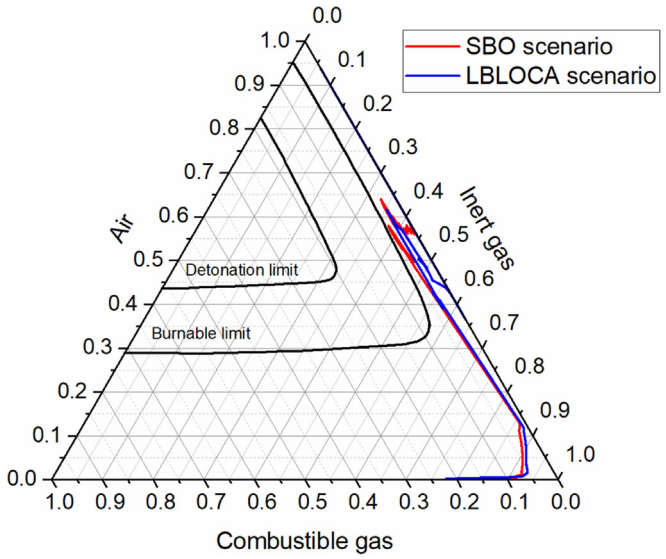

Fig. 13. Gas composition behavior in the containment for the case of 0.5 MPa opening pressure without PAR.

(2) The hydrogen risk was not affected by operation modes, whether to be continuous or cyclic operation. Only the first time when the CFVS opened there was a chance of hydrogen risk both for the cyclic and continuous operation modes. However, the cyclic operation enabled the CFVS availability longer. Therefore, it is better to operate CFVS in the cyclic mode for prolonged operation. Furthermore, according to the research of Lee et al. [19], the filtering performance decreases when the scrubbing pool is depleted. The pool can remain longer in the cyclic operating mode. Therefore, the cyclic operating mode is more effective than continuous operating mode from the viewpoint of reduction of release of radioactive materials as well.

(3) The effect of PAR was found significant. Without PAR, hydrogen risk appeared even when the CFVS operation pressure was set to be 0.5 MPa for which no hydrogen risk was found with PAR. Note that there was no hydrogen risk in the containment until the containment pressure went up to 0.5 MPa even without PAR. Therefore, the installation of PAR is crucial to reduce the hydrogen risk in the CFVS vessel prior to the containment.

The conclusions elucidated above were drawn from the two extreme accident scenarios; SBO and LBLOCA. SBO represents a slow progression case while LBLOCA does a fast progression one. Therefore, it could be said that the CFVS operation strategy suggested through this work would be applicable to a set of accidents between these two extreme cases. To develop a more detailed specific procedure for the CFVS operation, however, wide case studies with various accident scenarios are recommended.

Declaration of competing interest

The authors declare that they have no known competing financial interests or personal relationships that could have appeared to influence the work reported in this paper.

Acknowledgments

This research was supported by the Chung-Ang University Graduate Research Scholarship in 2020, the Nuclear Safety Research Program of the Korea Foundation of Nuclear Safety (KOFONS), with granted financial resources from the Nuclear Safety and Security Commission (NSSC) (Grant Code 1305008-0113-SB113) and a National Research Foundation of Korea (NRF) grant funded by the Korean government (MSIP: Ministry of Science, ICT and Future Planning) (No. NRF- 2017M2B2B1072552).

References

[1] D. Jacquemain, S. Guentay, S. Basu, M. Sonnenkalb, L. Lebel, H.J. Allelein, B. Liebana, B. Eckardt, L. Ammirabile, Status report on filtered containment venting, Organ. Econ. Co-Operation Dev. Energy Agency/Committee Saf. Nucl. Install. Paris, Fr. Fr. Rep. No. NEA/CSNI. 7 (2014).

[2] J. Yang, D.Y. Lee, S. Miwa, S. Chen, Overview of filtered containment venting system in nuclear power plants in Asia, Ann. Nucl. Energy 119 (2018) 87–97, https://doi.org/10.1016/j.anucene.2018.03.047.

[3] Y.M. Song, H.S. Jeong, S.Y. Park, D.H. Kim, J.H. Song, Overview of containment filtered vent under severe accident conditions at Wolsong Npp Unit 1, Nucl. Eng. Technol. 45 (2013) 597–604, https://doi.org/10.5516/net.03.2013.712.

[4] B. Eckardt, N. Losch, Filtered containment venting system designs, in: NRC Meet, Contain. Vent. Syst., 2012.

[5] S. Kawamura, T. Kimura, S. Omori, T. Narabayashi, Development of a filtered containment venting system for nuclear power plants, Trans. Atom. Energy Soc. Jpn. 15 (2015), https://doi.org/10.3327/taesj.J14.036.

[6] N.R. Lee, Y.S. Bang, D.Y. Lee, H.T. Kim, Analysis of containment venting strategy under severe accident conditions, Ann. Nucl. Energy 94 (2016) 633–642, https://doi.org/10.1016/j.anucene.2016.04.010.

[7] S. Schwarz, M. Sonnenkalb, Lessons Learned from Analytical Re-evaluation of a Venturi Scrubber Venting Systems Implemented in German NPPs through COCOSYS Analyses, International Atomic Energy Agency (IAEA), 2017. http://inis.iaea.org/search/search.aspx?orig_q=RN:48058113.

[8] T. Sevón, Molten core-concrete interactions in nuclear accidents, Espoo VTT Process, Notes 2311 (2005) 83.

[9] D. Macdonald, M. Urquidi-Macdonald, Y. Chen, J. Ai, P. Park, H.-S. Kim, Oxidation of Zircaloy Fuel Cladding in Water-Cooled Nuclear Reactors, The Pennsylvania State University, 2006.

[10] INTERNATIONAL ATOMIC ENERGY AGENCY, The Fukushima Daiichi Accident, 2015. Vienna, https://www.iaea.org/publications/10962/the-fukushima-daiichi-accident.

[11] Z. Liang, Status Report on Hydrogen Management and Related Computer Codes, Nuclear Energy Agency of the OECD (NEA), 2014. NEA-CSNI-R–2014-8.

[12] Y.S. Na, S.-W. Cho, K.S. Ha, The hydrogen issue in the initial operation of a filtered containment venting system, Nucl. Technol. 195 (2017) 329–334, https://doi.org/10.13182/nt15-160.

[13] M. Löffler, M. Braun, Evaluation of filtered containment venting systems with MELCOR for Extended operating conditions in German PWR, in: 6th Meet. "European MELCOR User Group", UJD, VUJE, Bratislava, Slovakia, 2014.

[14] Z. Ma, Y. Lu, R. Chen, H. Xiao, M. Wang, G.H. Su, S. Qiu, W. Tian, Study on the hydrogen risk in venturi scrubber filter of filtered containment venting system under PWR severe accident, Nucl. Eng. Des. 327 (2018) 61–69, https://doi.org/10.1016/j.nucengdes.2017.11.033.

[15] R.O. Gauntt, J.E. Cash, R.K. Cole, C.M. Erickson, L.L. Humphries, S.B. Rodríguez, M.F. Young, MELCOR Computer Code Manuals, NUREG/CR-6119, vol. 2, Sandia National Laboratories, Albuquerque, NM, USA, 2005. Rev. 3, SAND 2005-5713.

[16] T.W. Kim, S.J. Han, K. Il Ahn, Y.H. Jung, D. Fynan, Development and Application of source term analysis framework on OPR-1000 NPP for radiological emergency preparedness, 13th Int. Conf. Probabilistic Saf. Assess. Manag. (PSAM 13 (2016).

[17] Khnp, Hanul Unit 3,4 Final Safety Analysis Report, 1998.

[18] A. ENPRO C, Sartmadjiev, SAMG hydrogen related selected technical issues. Part III. Hydrogen distribution inside a WWER-1000 containment[development and validation of emergency operating procedures/accident management guidelines (EOP/AMG) for effective prevention/mitigation of Se, in: Nuclear Regulatory Authority of the Slovak Republic, 1999. Bratislava (Slovakia), Slovakia, https://www.osti.gov/etdeweb/servlets/purl/20067372.

[19] E.-H. Lee, H.-Y. Kim, J. Bang, D.-W. Jerng, T.W. Kim, Effects of the operating strategies of filtered containment venting system on Cesium-137 releases during severe accidents, Ann. Nucl. Energy 127 (2019) 469–478, https://doi.org/10.1016/j.anucene.2018.12.029.

[20] S.-W. Lee, T.-H. Hong, Y.-J. Choi, M.-R. Seo, H.-T. Kim, Containment depressurization capabilities of filtered venting system in 1000 MWe PWR with large dry containment, Sci. Technol. Nucl. Install. (2014) 1–10, https://doi.org/10.1155/2014/841895, 2014.

[21] T.W. Kim, S.J. Han, K.I. Ahn, D. Fynan, Y.H. Jung, Estimation of source term behaviors in SBO sequence in a typical 1000MWth PWR and comparison with other source term results, in: Proceedings of the KNS 2016 Spring Meeting, Republic of, Korea, 2016, 1CD-ROM.

[22] Y.S. Na, K.S. Ha, R.-J. Park, J.-H. Park, S.-W. Cho, Thermal hydraulic issues of containment filtered venting system for a long operating time, Nucl. Eng. Technol. 46 (2014) 797–802, https://doi.org/10.5516/net.02.2014.031.

[23] L. Gas, Lower and upper explosive limits for flammable gases and vapors (LEL/UEL), Matheson Gas Prod (2013) 22.

[24] Z.M. Shapiro, T.R. Moffette, Hydrogen Flammability Data and Application to PWR Loss-Of-Coolant Accident, Bettis Plant, Pittsburgh, PA (United States), 1957. Westinghouse Electric Corp.

[25] E.S.L.A. Conty, A Proposed Methodology for Passive Autocatalytic Recombiners Sizing and Location in LWR Containments, Universidad Politécnica de Madrid, 2016.